

Determinants of Ligand Binding Affinity and Cooperativity at the GLUT1 Endofacial Site

Trista Robichaud,[†] Antony N. Appleyard,[‡] Richard B. Herbert,[‡] Peter J. F. Henderson,[‡] and Anthony Carruthers^{*,†}

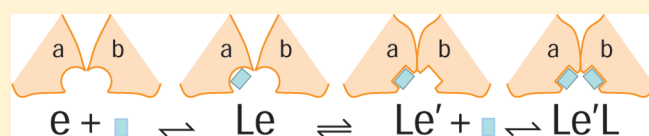
[†]Department of Biochemistry & Molecular Pharmacology, University of Massachusetts Medical School, 364 Plantation Street Worcester, Massachusetts 01605, United States

[‡]Astbury Centre, Institute of Membrane and Systems Biology, University of Leeds, Leeds LS2 9JT, U.K.

 Supporting Information

ABSTRACT: Cytochalasin B (CB) and forskolin (FSK) inhibit GLUT1-mediated sugar transport in red cells by binding at or close to the GLUT1 endofacial sugar binding site. Paradoxically, very low concentrations of each of these inhibitors produce a modest stimulation of sugar transport [Cloherty,

E. K., Levine, K. B., and Carruthers, A. (2001) The red blood cell glucose transporter presents multiple, nucleotide-sensitive sugar exit sites. *Biochemistry* 40 (51), 15549–15561]. This result is consistent with the hypothesis that the glucose transporter contains multiple, interacting, endofacial binding sites for CB and FSK. The present study tests this hypothesis directly and, by screening a library of cytochalasin and forskolin analogues, asks what structural features of endofacial site ligands determine binding site affinity and cooperativity. Like CB, FSK competitively inhibits exchange 3-O-methylglucose transport (sugar uptake in cells containing intracellular sugar) but noncompetitively inhibits sugar uptake into cells lacking sugar at 4 °C. This refutes the hypothesis that FSK binds at GLUT1 endofacial and exofacial sugar binding sites. Some forskolin derivatives and cytochalasins inhibit equilibrium [³H]-CB binding to red cell membranes depleted of peripheral proteins at 4 °C. Others produce a moderate stimulation of [³H]-CB binding when introduced at low concentrations but inhibit binding as their concentration is increased. Yet other analogues modestly stimulate [³H]-CB binding at all inhibitor concentrations applied. These findings are explained by a carrier that presents at least two interacting endofacial binding sites for CB or FSK. We discuss this result within the context of models for GLUT1-mediated sugar transport and GLUT1 quaternary structure, and we evaluate the major determinants of ligand binding affinity and cooperativity.



Cellular exchange of nutrients, ions, and metabolites proceeds via membrane-spanning proteins called channels and carriers.¹ The Major Facilitator Superfamily of carriers is responsible for the largest portion of nutrient transport in cells,² and among these carriers, the sugar porter subfamily is one of the oldest and largest family classifications.

Sugar porters catalyze both cellular sugar import and export, but net sugar transport always proceeds from high to low sugar concentration. The first human sugar transporter to be isolated was the erythrocyte membrane protein ¹GLUT1.^{3,4} GLUT1 is primarily expressed in the cardiovascular system and in astrocytes of the central nervous system and mediates glucose transport across blood–tissue barriers.⁵ Any one of several mutations in GLUT1 results in GLUT1 deficiency syndrome (GLUT-1DS) in which reduced glucose transport into the brain leads to developmental defects and seizures.⁶

Hydropathy analysis, scanning glycosylation mutagenesis, and proteolytic digestion studies confirm that GLUT1 (a 55 kDa protein) contains 12 α-helical transmembrane domains.⁷ Each GLUT1 polypeptide is thought to function as a simple carrier,⁸ presenting either a sugar uptake (exofacial) or a sugar exit (endofacial) site at any given moment. However, this proposed transport mechanism does not explain the behavior

of GLUT1 in human red cells⁹ where GLUT1 monomers self-associate into cooperative oligomers, simultaneously exposing exofacial and endofacial binding sites and displaying a litany of catalytic behaviors incompatible with the simple carrier mechanism.¹⁰

Scanning cysteine mutagenesis analysis¹¹ suggests that the GLUT1 sugar uptake site involves portions of α-helical, transmembrane spanning regions 1, 5, 7, 8, and 11. Peptide mapping studies of affinity labeled GLUT1 suggest that the exit site contains a subdomain of membrane spanning regions 10 and 11.¹² However, specific GLUT1 residues contacting glucose in GLUT1 exofacial (e2) and endofacial (e1) conformations are unknown.

The present study characterizes the GLUT1 export conformation by analysis of inhibitor binding to the e1 conformer. Comprehensive analysis of GLUT1 interaction with a library of inhibitors may reveal details of the complementary relationship between ligand and binding pocket structures. We selected GLUT1 endofacial site inhibitors and their derivatives for this analysis. Cytochalasin B (CB) is a cell-permeable alkaloid that disrupts

Received: December 21, 2010

Revised: March 7, 2011

Published: March 08, 2011

actin filaments and inhibits glucose transport.¹³ Forskolin (FSK) is a cell-permeable diterpenoid that inhibits GLUT1 and activates adenylate cyclase.¹⁴ Both CB and FSK are thought to bind to the endofacial orientation of GLUT1 where they act as noncompetitive inhibitors of erythrocyte glucose uptake and competitive inhibitors of exit.^{14,15} These endofacial inhibitors have also been docked to an homology-based, theoretical GLUT1 structure where they are proposed to bind to cytoplasmic domains of the carrier.¹⁶ Our findings confirm that endofacial, export-site inhibitors inhibit ligand binding by two mechanisms—direct competition and cooperative inhibition—and provide new insights into the molecular determinants of each type of inhibition.

MATERIALS AND METHODS

Solutions. Kaline consisted of 150 mM KCl, 5 mM MgCl₂, 5 mM EGTA, 5 mM HEPES, pH 7.4. Lysis buffer contained 10 mM Tris-HCl, 2 mM EDTA, pH 8.0. Stripping solution contained 2 mM EDTA, 15.4 mM NaOH, pH 12. Sugar-stop solution consisted of ice-cold Kaline containing 20 μ M CB and 200 μ M phloretin.

Materials. [³H]-3-O-Methylglucose, [³H]-cytochalasin B, and [³H]-forskolin were purchased from Sigma Chemicals. Human blood was purchased from Biological Specialty Corp. Forskolin derivatives were synthesized by A. N. Appleyard. Other reagents were purchased from Sigma Chemicals.

Red Cells. Red cells were isolated from whole human blood by centrifugation as described previously.⁹

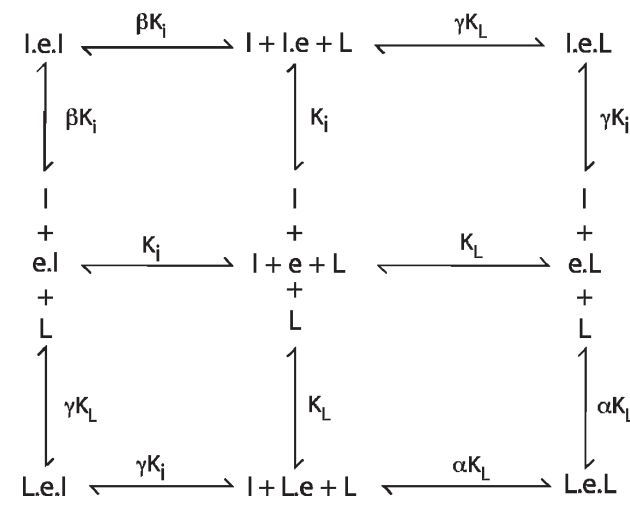
Red Cell Membranes. Red cell membranes depleted of peripheral membrane proteins (including the cytochalasin B binding protein actin) were prepared as described in ref 17.

3-O-Methylglucose Uptake. Zero trans 3MG uptake (3MG uptake into cells lacking intracellular sugar) and equilibrium exchange 3MG sugar uptake (unidirectional [³H]-3MG uptake in cells where intracellular [3MG] = extracellular [3MG]) were measured at 4 °C as described previously.^{9,18}

Forskolin or Cytochalasin B Inhibition of 3OMG Transport. 3MG uptake was measured as described above in the absence and presence of cytochalasin B, forskolin, or their derivatives. Inhibitor concentrations ranged from 10^{−9} to 10^{−4} M using ethanol or dimethyl sulfoxide as solvents. Solvent concentration never exceeded 0.1% (vol:vol) and is without effect on sugar transport rates. Cells were preincubated with inhibitor for 15 min on ice before starting uptake measurements. When transport inhibition was profound (>75%), the uptake interval was extended to permit more accurate determinations of uptake.

Ligand Binding Competition Assay. Stripped ghosts (peripheral protein-depleted membranes) were diluted to 2 mg/mL in 50 mM Tris medium, pH 7.4 at 4 °C. Ligand binding assay solutions comprised Tris medium plus 50 nM unlabeled CB, 14 μ Ci [³H]-CB plus a range of inhibitor (I) concentrations (0–100 μ M). Some ligand binding assays substituted 50 nM forskolin and 34 μ Ci [³H]-forskolin for cytochalasin B. Binding assays were as described previously.¹⁹ Membranes (50 μ L) and ligand binding solutions (50 μ L) were mixed in a microcentrifuge tube, and following 15 min of inversion at 4 °C, two 10 μ L aliquots were sampled (Total dpms). The tubes were centrifuged at 14 000 rpm for 5 min, and two 10 μ L aliquots of the supernatant were sampled (Free dpms). “Bound” dpms were calculated as the difference between “total” and “free”

Scheme 1



dpms. Each inhibitor concentration was tested three times in triplicate.

LIGAND BINDING TO GLUT1: THEORY

Assay by Ligand Depletion. The nature of the binding assay adds a significant complication to the analysis. This is a ligand depletion assay in which [GLUT1] \approx 1–2 μ M, radiolabeled CB or FSK (L_{total}) is 50 nM, and competing (unlabeled ligand, I) ranges from 0 to 50 μ M. Thus, at low [I]_{total}, the concentration of [I]_{free} < [I]_{total} due to binding to GLUT1. [L]_{free} and [L]_{bound} are always measured directly. Errors in determination of K_i , β , and γ derive from the assumption [I]_{total} = [I]_{free} when $K_i \leq$ [GLUT1].

Even after allowing for ligand depletion as above, equilibrium cytochalasin B and forskolin binding to GLUT1 display non-Michaelis kinetics at low ligand concentrations.^{20–22} The simplest model that accounts for this behavior (see Scheme 1) assumes that the glucose transporter complex presents two interacting binding sites for endofacial ligands. This could be explained either by two sites on one transport protein or two interacting transport proteins each with one site. When presented with a binary mixture of ligands (e.g., radio-ligand L plus inhibitor I), the transporter, e, may form several liganded states (see Scheme 1): e (unliganded transporter), 2(I.e), 2(L.e), 2(I.e.L), L.e.L, and I.e.I.

When measuring CB binding in the presence of FSK, binding of the first CB molecule to unoccupied GLUT1 is described by the dissociation constant K_L and binding of the second CB molecule is described by αK_L , where α is a dimensionless constant greater than zero. Binding of the first FSK molecule to unoccupied transporter is described by K_i , and binding of the second FSK molecule is described by βK_i (β is a dimensionless constant greater than zero). When heterocomplexes are formed, binding of the first molecule (CB or FSK) is described by K_L or K_i and binding of the second molecule (FSK or CB) is described by γK_L or γK_i , where γ is a dimensionless constant greater than zero. This model explains enhanced CB binding in the presence of at least 11 of the 20 “antagonists” tested in the present study. Cooperative interactions between binding sites (positive or negative cooperativity) may depend on whether the first and

second ligands to bind are identical or different. For example, the ligand CCB might reduce binding of the remaining site for CCB ($\alpha > 1$; negative homocooperativity) but increase the affinity of the remaining site for inhibitor I ($\gamma < 1$; positive heterocooperativity), or vice versa.

Equilibrium ligand binding (L_b) to GLUT1 in the presence of a competing e1 inhibitor I is described by

$$L_b = \frac{B_{\max}L}{K_{d(\text{app})} + L} \quad (1)$$

where B_{\max} is given by

$$[e] \frac{2 \left(1 + \frac{L}{\alpha K_L} + \frac{I}{\gamma K_I} \right)}{2 + \frac{L}{\alpha K_L} + \frac{2I}{\gamma K_I}} \quad (2)$$

$K_{d(\text{app})}$ is given by

$$\frac{K_L \left(1 + \frac{I}{K_I} \left\{ 2 + \frac{1}{\beta K_I} \right\} \right)}{2 + \frac{L}{\alpha K_L} + \frac{2I}{\gamma K_I}} \quad (3)$$

when $I = 0$

$$B_{\max} = 2[e] \frac{\alpha K_L + L}{2\alpha K_L + L} \quad (4)$$

$$K_{d(\text{app})} = \frac{K_L}{2 + \frac{L}{\alpha K_L}} \quad (5)$$

where K_L , K_I , α , β , and γ are shown in Scheme 1. Since B_{\max} does not include I terms, inhibitor I does not affect B_{\max} for L binding to GLUT1. The ratio CB binding in the presence of inhibitor:CB binding in the absence of inhibitor (b_i/b) is thus given by

$$\begin{aligned} \frac{b_i}{b} = & \frac{[\beta K_I \{ \alpha K_L (I + \gamma K_I) + \gamma K_I L \} \{ L^2 + \alpha K_L (K_L + 2L) \}]}{[(\alpha K_L + L) \{ \beta \gamma K_I^2 L^2 + \alpha K_L (I^2 \gamma K_L + 2\beta K_I I (\gamma K_L + L) \\ & + (\beta \gamma K_I^2 (K_L + 2L)) \}]} \end{aligned} \quad (6)$$

When cytochalasin B (I) inhibition of [^3H]-cytochalasin B (L) binding (or forskolin (I) inhibition of [^3H]-forskolin (L)) is measured, the analysis simplifies considerably because $\alpha = \beta = \gamma$ and $K_L = K_I$. Equation 6 simplifies to

$$\frac{b_i}{b} = \frac{(\alpha K_L + L + I)(L^2 + \alpha K_L (K_L + 2L))}{(\alpha K_L + L)(I^2 + L^2 + 2I(\alpha K_L + L) + \alpha K_L (K_L + 2L))} \quad (7)$$

I and L are measured directly from the raw binding data, so the homoinhibition experiment allows the unambiguous calculation of K_L and α for cytochalasin B and forskolin (Table 1).

This analysis assumes that all binding and dissociation steps are rapid relative to the duration of experimental measurement and that free and bound ligand achieve true equilibrium. These assumptions are most likely satisfied because cytochalasin B binding to GLUT1 occurs with a time constant of 1 s at 4 °C,^{10,23} whereas binding was measured over a period of 15 min (>1000 half-lives). The model allows for several possible effects of inhibitor (I) on ligand (L) binding.

1. *Binding is not cooperative.* When binding of L and I at any single site is mutually exclusive and lacks heterocooperativity ($\gamma = 1$; Figure 1, curve a), the inhibitor I will serve as a simple competitive inhibitor of L binding.
2. *Binding is negatively cooperative.* When binding of L and I at any single site is mutually exclusive and displays negative heterocooperativity ($\gamma > 1$; Figure 1, curve b), the inhibitor I will appear to serve as a simple competitive inhibitor of L binding although the inhibition dose response is shifted to the left.
3. *Binding is positively cooperative.* When binding of L and I at any single site is mutually exclusive but displays positive heterocooperativity between sites ($\gamma < 1$; Figure 1, curve c), the inhibitor I will enhance L binding at low [I] where I and L bind at adjacent sites. When [I] is increased further such that I and L compete for binding to the same site, L binding is inhibited.
4. *Zero heterocooperativity and positive or negative homocooperativity.* When binding of L and I at any single site is mutually exclusive but displays zero heterocooperativity and positive homocooperativity (i.e., $\beta < 1$ and $\gamma = 1$; Figure 1, curve d), the inhibitor I will inhibit L binding more effectively (the inhibition curve is left-shifted). If the inhibitor I displays negative homocooperativity, I will be a less effective inhibitor and maximum inhibition will be reduced (i.e., $\beta > 1$ and $\gamma = 1$; Figure 1, curve e).
5. *Positive heterocooperativity and positive or negative homocooperativity.* When binding of L and I at any single site is mutually exclusive but displays positive heterocooperativity and positive homocooperativity (i.e., $\beta \ll 1$ and $\gamma \ll 1$; Figure 1, curve f), the inhibitor I will enhance L binding at low [I] and inhibit binding at greater [I]. If the inhibitor I displays negative homocooperativity ($\beta \gg 1$) but strong positive heterocooperativity ($\gamma \ll 1$), I will enhance ligand binding at all [I] (Figure 1, curve g).

Data Analysis. Having measured K_L and α from analyses of CB inhibition of [^3H]-CB binding or forskolin inhibition of [^3H]-forskolin binding (eq 7), the analytical cycle is as follows:

- (1) Compute initial estimates of K_b , β , and γ by nonlinear regression analysis of b_i/b (experimental) vs [I]_{total} using eq 6.
- (2) Using these parameter estimates, compute [I]_{free} using Berkeley Madonna (version 8.3.22)—a general purpose differential equation solver that assumes [I] \approx [GLUT1] and thus allows [I]_{free} to fall as I interacts with GLUT1. The details of the model (differential equations describing Scheme 1) are available in the Supporting Information.
- (3) Using these estimates of [I]_{free}, recompute K_b , β , and γ by nonlinear regression of b_i/b (experimental) vs computed [I]_{free} using eq 6.
- (4) Using these values of newly computed K_b , β , and γ , compare plots of b_i/b (theoretical) vs [I]_{total} to b_i/b (experimental) vs [I]_{total} by calculating the sum of the squares of deviations of theoretical data from experimental data.

Repeat steps 2 through 4 until the sum of the squares of deviations of b_i/b (theoretical) vs [I]_{total} from b_i/b (experimental) vs [I]_{total} is minimized.

RESULTS

Cytochalasin B is a competitive inhibitor of equilibrium exchange transport in erythrocytes²⁴ and a noncompetitive inhibitor of net sugar uptake into red cells lacking sugar.¹⁵ Equilibrium exchange transport is a condition in which intra- and extracellular

Table 1. Modulation of Cytochalasin B Binding to Red Cell Membranes by Cytochalasins and Forskolins: Summary of Findings^a

ligand ^b	K_L , ^c nM	α ^d	K_b , ^e nM	ΔG° , ^f kcal/mol	$\Delta\Delta G^\circ$, ^g kcal/mol	β ^h	γ ^h	R^2 ^h	inhibition ⁱ	βK_b , ^j nM	γK_b , ^j μ M	$ss^* \gamma$ ^j
CCB	98 ± 8.5	6.28 ± 3.85	98 ± 8.5	−8.88		6.28 ± 3.85	6.28 ± 3.85	0.99	1	616	616	39
CCA			815 ± 96	−7.72	1.17	1.11 ± 0.17	0.374 ± 0.052	1.00	2	905	302	0.42
CCH			98 ± 3	−8.88	0.00	249 ± 45	0.449 ± 0.019	0.94	2	24 402	44	110
CCJ			12 ± 1	−10.04	−1.16	6399 ± 347	0.635 ± 0.013	0.99	3	76 788	8	4063
CCD			1969 ± 98	−7.23	1.65	101 ± 61	0.557 ± 0.019	0.98	3	198 869	1097	51
CCE			99 ± 8	−8.88	0.01	7917 ± 2935	0.555 ± 0.016	0.96	3	783 783	55	4394
CCC			1591 ± 431	−7.35	1.53	∞	0.433 ± 0.003	0.99	4	∞	689	∞
FSK	2750 ± 787	2.43 ± 0.23	3282 ± 960	−6.95		1.54 ± 0.73	0.930 ± 0.103	0.93	1	5 054	3052	1
1415DiHFSK			29.1 ± 17	−9.55	−2.60	242.7 ± 140	0.571 ± 0.015	0.99	1	7 042	17	139
6AFSK			949 ± 164	−7.63	−0.68	9.84 ± 0.68	0.416 ± 0.019	0.95	2	9 338	389	4
1,6DiAFSK			11 ± 2	−6.28	0.67	1480 ± 268	0.489 ± 0.017	0.94	2	16 280	5	724
1DOFSK			1.0 ± 0.7	−11.41	−4.46	22179 ± 5104	0.438 ± 0.017	0.97	2	22 179	0.4	9714
7FAFSK			629 ± 644	−7.86	−0.91	45.3 ± 5.0	0.475 ± 0.010	0.97	2	28 494	296	22
1AFSK			3 ± 2	−10.80	−3.85	11923 ± 8441	0.440 ± 0.008	0.86	2	35 769	1	5246
9DOFSK			430 ± 75	−8.07	−1.12	120.3 ± 12.3	0.464 ± 0.016	0.75	2	51 729	198	56
7PFAFSK			142 ± 78	−4.88	2.07	1115 ± 218	0.508 ± 0.012	0.65	3	158 330	71	566
7FPPNeaFSK			25 ± 8.4	−9.63	−2.68	40416 ± 1646	0.430 ± 0.086	0.74	4	1 010 400	11	17 379
7DeAFSK			2 ± 2	−11.02	−4.07	∞	0.450 ± 0.008	0.86	4	∞	1	∞
6A7DeAFSK			NA ^l			NA ^l	NA ^l	NA ^l	5			
7FPPFSK			NA ^l			NA ^l	NA ^l	NA ^l	5			
						mean ^k	0.493 ± 0.056					

^a The results of analyses such as those in Figures 3, 4, and 5 are summarized for the cytochalasins and the forskolins. The concentration of radio-ligand (³H)-CB was 50 nM in all experiments. ^b The total concentration of unlabeled competing ligand was varied from 0 to 100 μ M. Analysis of binding inhibition was carried out as described in Figures 2 and 3 using eqs 6 and 7 and the iterative analysis procedure outlined in the Materials and Methods. ^c K_L (nM) for CB was computed in studies of CB inhibition of [³H]-CB binding and assume that $\alpha = \beta = \gamma$. ^d α for FSK binding was computed in studies of FSK inhibition of [³H]-FSK binding and assume that $\alpha = \beta = \gamma$. ^e K_I (nM) represents the affinity of unoccupied GLUT1 for ligand. ^f ΔG° was calculated as $RT \ln(1/K_I)$. ^g $\Delta\Delta G^\circ$ was calculated as the change in ΔG° using the lowest K_I for cytochalasins or forskolins as the baseline. ^h Analysis according to eq 6 also permits computation of the cooperativity parameters β and γ and yields a correlation coefficient R^2 . ⁱ Types of inhibition are: 1, Michaelis-like inhibition (curves a and e, Figure 1); 2, stimulation followed by inhibition (curves c and f, Figure 1); 3, high and low affinity inhibition (curve d, Figure 1); 4, stimulation (curve g, Figure 1); 5, no effect. ^j These types of inhibition are unrelated to the products βK_b , γK_b , or $\beta\gamma$. ^k While β parameters are ligand-dependent, γ parameters appear to be invariant and are averaged for the cytochalasins and forskolins (mean \pm SEM). ^l No effect on binding was observed. In all experiments, at least three (normally four) complete dose responses were performed with each data point in triplicate. The 9 or 12 data points were then averaged at each concentration to perform the final analysis.

[sugar] are identical and unidirectional fluxes are monitored through use of tracer sugar. Competitive inhibition by cytochalasin B indicates that extra- or intracellular sugar compete with cytochalasin B for binding to the transporter. Noncompetitive inhibition of uptake into cells lacking sugar indicates the absence of competition between extracellular sugar and inhibitor at the uptake site. This aggregate behavior is characteristic of an inhibitor that binds at (or whose binding site is mutually exclusive with) the endofacial sugar-binding site.¹⁵

Forskolin is a competitive inhibitor of cytochalasin B binding to the human erythrocyte sugar transporter²⁵ suggesting that forskolin, like cytochalasin B, binds at or close to the transporter endofacial site. In support of this hypothesis, we observe that forskolin acts as a noncompetitive inhibitor of net sugar uptake (Figure 2A) and as a competitive inhibitor of exchange sugar uptake (Figure 2B) in human erythrocytes. Forskolin reduces V_{\max} for sugar uptake by sugar-depleted cells but increases $K_{m(\text{app})}$ for equilibrium exchange transport. Assuming noncompetitive and competitive inhibition of 3MG zero-trans and equilibrium exchange transport, respectively, $K_{i(\text{app})}$ for FSK inhibition of net and exchange transport are 1.9 ± 0.4 and $1.2 \pm 0.6 \mu\text{M}$, respectively.

We screened the ability of forskolin and its derivatives to displace cytochalasin B from GLUT1 by measuring forskolin inhibition of equilibrium ³H-cytochalasin B binding to red cell membranes depleted of peripheral membrane proteins. Cytochalasin B binding to peripheral membrane protein-depleted human red cell membranes is competitively displaced by D-glucose

and other GLUT1 substrates and is quantitatively accounted for by ligand binding to GLUT1.^{26,27}

Quantitation of inhibition of nM levels of ³H-cytochalasin B binding to μM concentrations of GLUT1 by mM levels of sugars is quite straightforward. However, the ligand binding assay employed in the current study is a “radioligand depletion” assay (see Materials and Methods). Specifically, we measure total [radioligand] in a suspension of GLUT1 proteoliposomes, and following sedimentation of GLUT1 proteoliposomes by centrifugation, we measure free [radioligand] remaining in the supernatant. Bound [radioligand] is thus total—free [radioligand]. By necessity, the concentration of GLUT1 used in these studies must deplete free [radioligand] sufficiently to produce a measurable difference between total and free [radioligand]. If a non-radiolabeled inhibitor also binds to GLUT1 to deplete free [inhibitor], then plots of equilibrium bound [radioligand] versus total [inhibitor] do not reflect the free [inhibitor] that produces inhibition of radioligand binding. Since radiolabeled inhibitors are, in most instances, unavailable, it is often impossible to measure free [inhibitor] directly. The net effect is that the use of radioligand depletion assays, in which bound [radioligand] is expressed as a function of total [inhibitor], inevitably overestimate K_I for inhibition of radioligand binding by inhibitor. This is illustrated in measurements of inhibition of [³H]-CB binding to GLUT1 by non-radiolabeled CB (Figure 3A) and by measurements of inhibition of [³H]-forskolin binding to GLUT1 by non-radiolabeled forskolin (Figure 3B).

CB binding to GLUT1 is a relatively high affinity process with $K_{d(\text{app})} \approx 100$ nM. CB is also available in radiolabeled ([³H]-CB)

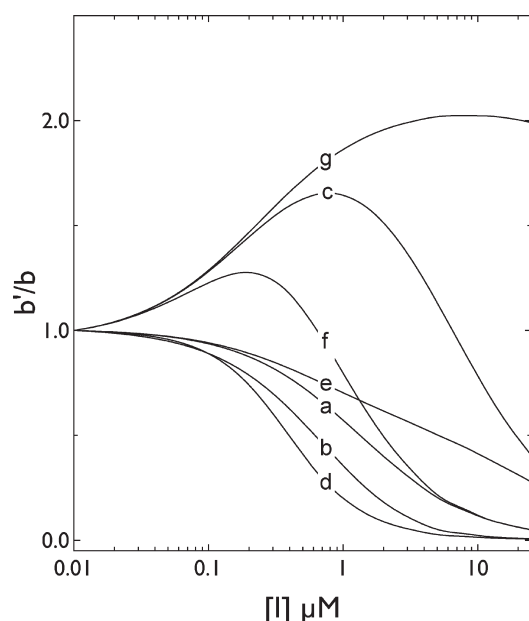


Figure 1. Simulations of effects of inhibitors on cytochalasin B binding to GLUT1 when each transporter complex contains two interacting binding sites. Ordinate: CB binding in the presence of an inhibitor/CB binding in the absence of inhibitor (calculated using eq 5). Abscissa: inhibitor concentration in μM (note the log scale). Seven (a–g) scenarios were simulated. In each instance K_L for CB binding, K_i for inhibitor binding, and α (cooperativity between CB binding sites when only the CB is present) were set at $0.25 \mu\text{M}$, $1 \mu\text{M}$, and 1, respectively. The curves show (a) $\beta = \gamma = 1$; (b) $\beta = 1, \gamma = 10$; (c) $\beta = 1, \gamma = 0.1$; (d) $\beta = 0.1, \gamma = 1$; (e) $\beta = 10, \gamma = 1$; (f) $\beta = \gamma = 0.1$; (g) $\beta = 100, \gamma = 0.1$.

and non-radiolabeled ($[^1\text{H}]$ -CB) forms. This permits direct measurements of bound and free [CB] as outlined above. Thus, when CB binding is measured as the ratio of binding in the presence of unlabeled CB to binding in the absence of unlabeled CB, or b_i/b , and is expressed as a function of total or free [CB], two observations are apparent. (1) The curve describing b_i/b versus [CB] is significantly right-shifted when total [CB] is used versus free [CB]. (2) The curve fit is significantly better when using free [CB].

A third data set is shown in Figure 3A. This data set shows measured b_i/b versus simulated free [CB]. Simulated free [CB] was obtained through a multistep process: (1) We computed binding parameters (K_L and α , see eq 7) by using the b_i/b versus total [CB] data. (2) Using these parameters, we then simulated CB binding to GLUT1 under conditions where total [CB] and [GLUT1] are identical to those used experimentally. Our simulations used a general purpose differential equation solver (Berkeley Madonna) that recognizes $[\text{CB}] \approx [\text{GLUT1}]$ and thus allows $[\text{CB}]_{\text{free}}$ to fall as CB interacts with GLUT1. The details of the model (differential equations describing Scheme 1) are available in the Supporting Information. The output includes equilibrium CB binding and free [CB] at each total [CB] employed. (3) Measured CB binding is then plotted versus simulated free [CB], and K_L and α are recalculated. (4) We calculate the deviation between measured and simulated binding at each total [CB] and then square and sum these deviations. (5) Steps 2–4 are repeated until the sum of the square of the deviations no longer changes significantly. The result is two binding isotherms which accurately reproduce the plots of b_i/b

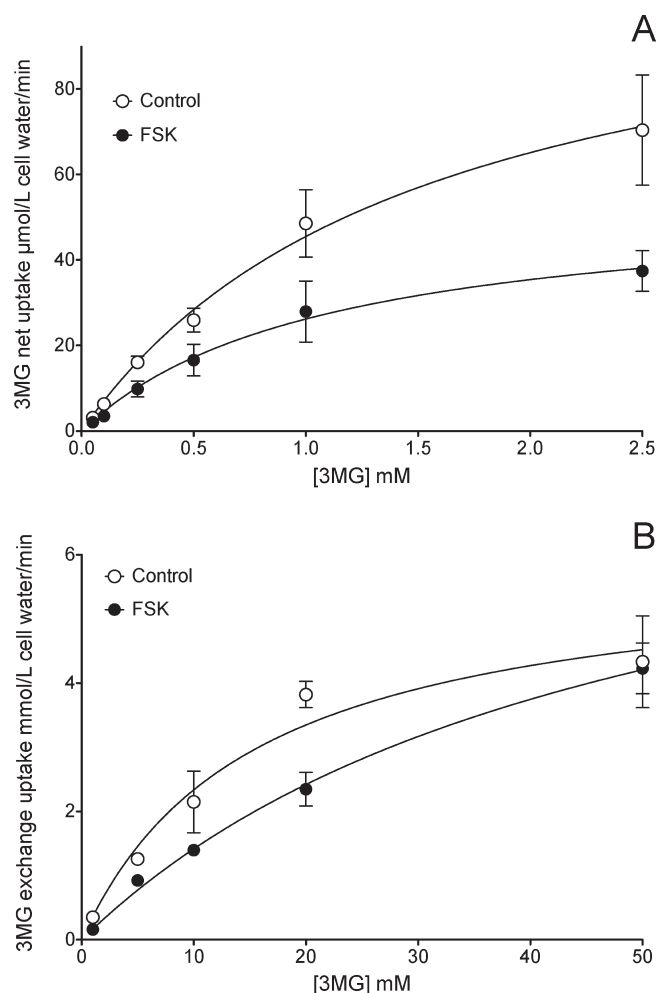


Figure 2. Inhibition of erythrocyte sugar transport by forskolin. Panels A and B: Ordinate: initial rate of 3MG uptake (mmol/L cell water/min). Abscissa: [3MG] mM. Results are shown as mean \pm SEM of at least three experiments made in quadruplicate. Uptake was measured in the absence (○) and presence (●) of $2 \mu\text{M}$ FSK. Curves drawn through the points were computed by nonlinear regression assuming that 3MG uptake follows simple Michaelis–Menten kinetics. (A) Zero-trans 3MG uptake (cells lack intracellular sugar). Control: $K_{\text{mapp}} = 1.51 \pm 0.22 \text{ mM}$; $V_{\text{max}} = 0.114 \pm 0.009 \text{ mM}/(\text{L min})$; $R^2 = 0.995$. FSK: $K_{\text{mapp}} = 1.09 \pm 0.15 \text{ mM}$; $V_{\text{max}} = 0.055 \pm 0.004 \text{ mM}/(\text{L min})$, $R^2 = 0.994$. (B) Equilibrium-exchange 3MG uptake (intracellular [sugar] = extracellular [sugar]). Control: $K_{\text{mapp}} = 17.8 \pm 4.7 \text{ mM}$; $V_{\text{max}} = 6.5 \pm 0.7 \text{ mM}/(\text{L min})$, $R^2 = 0.981$. FSK: $K_{\text{mapp}} = 48.5 \pm 7.3 \text{ mM}$; $V_{\text{max}} = 8.3 \pm 0.7 \text{ mM}/(\text{L min})$, $R^2 = 0.997$.

versus free [CB] and b_i/b versus total [CB]. Similar results are obtained with assays of forskolin inhibition of $[^3\text{H}]$ -forskolin binding to GLUT1 (Figure 3B) although the binding measurements show more experimental variation because K_d for forskolin binding to GLUT1 is at least 20-fold greater than K_d for CB binding. A second consequence of the higher K_d for forskolin binding is that the curves are significantly less left-shifted when b_i/b is plotted as a function of measured or simulated free [forskolin] versus total [forskolin].

These computations provide an iterative process for accurately estimating free [inhibitor] when a radiolabeled form of inhibitor is unavailable. Tests for internal consistency mandate that studies of unlabeled forskolin inhibition of $[^3\text{H}]$ -forskolin binding to GLUT1 (forskolin homoinhibition) provide binding constants that are

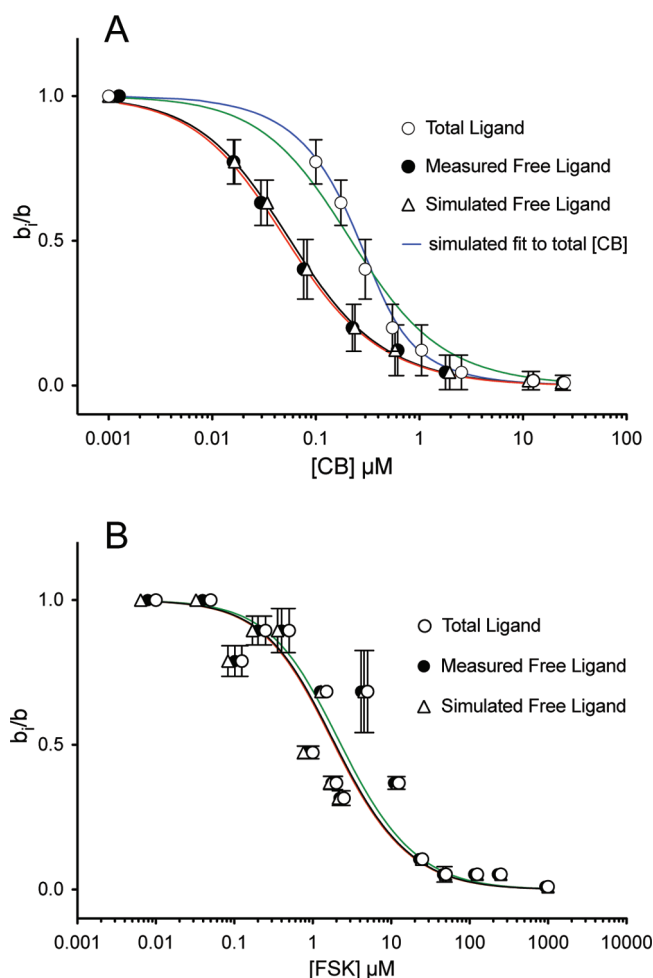


Figure 3. Modulation of $[^3\text{H}]\text{-CB}$ binding to red cell membranes by CB (A) and modulation of $[^3\text{H}]\text{-FSK}$ binding to red cell membranes by FSK (B). Ordinate: the ratio radioligand binding in the presence of inhibitor to radioligand binding in the absence of inhibitor. Abscissa: $[\text{inhibitor}]$, μM (note the log scale). Results are shown as mean \pm SEM of at least three separate measurements made in triplicate. Radioligand binding was measured at 50 nM total $[^3\text{H}]\text{-CB}$ or $[^3\text{H}]\text{-FSK}$. Results are shown for inhibition versus total $[\text{inhibitor}]$ (\circ), inhibition versus measured free $[\text{inhibitor}]$ (\bullet), and inhibition versus computed free $[\text{inhibitor}]$ (Δ). Curves drawn through the points were computed by nonlinear regression using eq 7. (A) The results for CB inhibition of $[^3\text{H}]\text{-CB}$ binding are $K_i = 0.408 \pm 0.178$ (total CB), 0.098 ± 0.014 (measured free CB), and 0.101 ± 0.009 (simulated free CB) μM ; $\alpha = 10.0 \pm 1.0$ (total CB), 5.441 ± 0.558 (measured free CB), and 7.01 ± 0.53 (simulated free CB). The black curve shows the computed best fit of b_i/b vs measured free $[\text{CB}]$. The red curve shows the computed best fit of b_i/b vs simulated free $[\text{CB}]$. The blue curve shows the computed best fit of b_i/b vs total $[\text{CB}]$ resulting from the simulations. The green curve shows the computed best fit of b_i/b vs free $[\text{CB}]$ assuming that free $[\text{CB}] = \text{total } [\text{CB}]$. (B) The results for FSK inhibition of $[^3\text{H}]\text{-FSK}$ binding are $K_i = 3.329 \pm 0.893$ (total FSK), 2.833 ± 0.754 (measured free FSK), and 2.750 ± 0.787 (simulated free FSK) μM ; $\alpha = 2.383 \pm 2.116$ (total FSK), 2.400 ± 0.212 (measured free FSK), and 2.434 ± 0.235 (simulated free FSK). The black curve shows the computed best fit of b_i/b vs measured free $[\text{FSK}]$. The red curve shows the computed best fit of b_i/b vs simulated free $[\text{FSK}]$. The green curve shows the computed best fit of b_i/b vs free $[\text{FSK}]$ assuming that free $[\text{FSK}] = \text{total } [\text{FSK}]$. Note the black and red curves are almost superimposable.

indistinguishable from analogous constants for forskolin modulation of $[^3\text{H}]\text{-cytochalasin B}$ binding (heteroinhibition, see Figure 4 and Table 1). As we will show, this is observed experimentally.

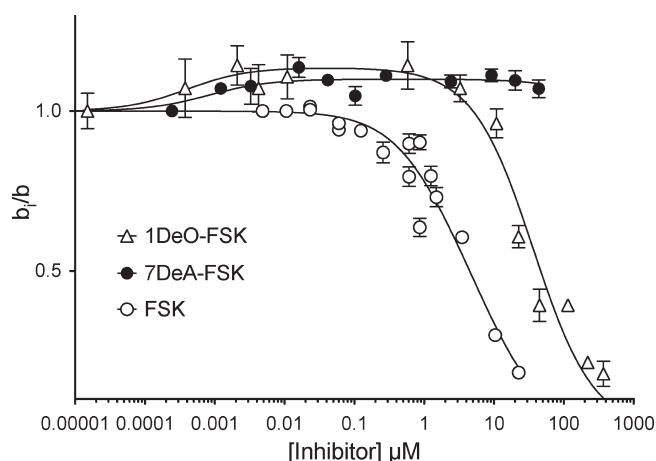


Figure 4. Modulation of $[^3\text{H}]\text{-CB}$ binding to red cell membranes by forskolin and its derivatives. Ordinate: the ratio CB binding in the presence of forskolin to CB binding in the absence of forskolin. Abscissa: $[\text{forskolin}]$, μM (note the log scale). Results are shown as mean \pm SEM of at least three separate measurements made in triplicate. CB binding was measured at 50 nM $[^3\text{H}]\text{-CB}$. Results are shown for inhibition by FSK (\circ), 7DAFSK (\bullet) or 1DOFSK (Δ). Curves drawn through the points were computed by nonlinear regression using eq 6. Based on CB inhibition of $[^3\text{H}]\text{-CB}$, K_i and α were set at $0.098 \pm 0.085 \mu\text{M}$ and 6.284 ± 0.558 , respectively. The results are: FSK, $K_i = 3.28 \pm 0.98 \mu\text{M}$, $\beta = 1.54 \pm 0.73$, $\gamma = 0.93 \pm 0.10$, $R^2 = 0.93$. 7DeA-FSK, $K_i = 2 \pm 2 \text{ nM}$, $\beta = \infty$, $\gamma = 0.45 \pm 0.01$, $R^2 = 0.86$. 1DO-FSK, $K_i = 1.0 \pm 0.7 \text{ nM}$, $\beta = 22179 \pm 5104$, $\gamma = 0.438 \pm 0.017$, $R^2 = 0.97$.

Forskolin and its derivatives modify $[^3\text{H}]\text{-cytochalasin B}$ (50 nM) binding to GLUT1 in several interesting ways (Figure 4 and Table 1). Some forskolins appear to function as simple inhibitors of cytochalasin B binding in which inhibition is a saturable function of $[\text{forskolin}]$. Other forskolins (see Figure 4 and Table 1) first enhance and then inhibit cytochalasin B binding as the concentration of the inhibitor is raised. Yet other inhibitor analogues simply increase cytochalasin B binding (see Figure 4 and Table 1) while others appear to be without effect.

These behaviors are predicted by a simple binding model (Scheme 1) in which each transporter complex presents two cytochalasin B or forskolin binding sites that interact in ways that are dependent upon the nature of the bound ligands. For example, if binding of a forskolin derivative at the first site increases the affinity of the second site for cytochalasin B or the forskolin derivative, cytochalasin B binding may be enhanced at low $[\text{forskolin}]$ and then inhibited as $[\text{forskolin}]$ is raised and competes more effectively with cytochalasin B for binding at the second site. Other permutations are possible (see Scheme 1 and Figure 1), and according to the model, the net effect of any $[\text{forskolin}]$ on cytochalasin B binding is determined by five parameters: K_L (K_d for cytochalasin B binding), K_I (K_d for forskolin derivative binding), α (a cooperativity factor indicating how cytochalasin B binding at the first site impacts $K_{d(\text{app})}$ for cytochalasin B binding at the second site), β (a cooperativity factor indicating how forskolin binding at the first site impacts $K_{d(\text{app})}$ for forskolin binding at the second site), and γ (a cooperativity factor indicating how cytochalasin B binding at the first site impacts $K_{d(\text{app})}$ for forskolin binding at the second site). In homoinhibition studies where, for example, the radioligand and unlabeled competing ligand are the same species (e.g., cytochalasin B or forskolin), $K_L = K_I$ and $\alpha = \beta = \gamma$, thereby simplifying analysis of experimental data to the resolution of two affinity

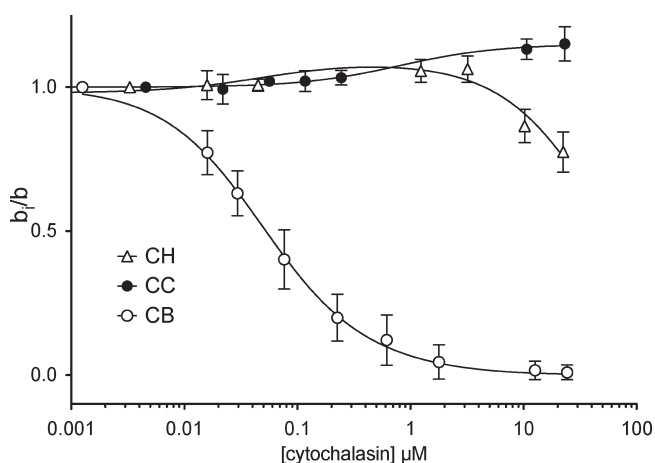


Figure 5. Modulation of [^3H]-cytochalasin B binding to red cell membranes by cytochalasins. Ordinate: the ratio [^3H]-CB binding in the presence of other cytochalasins to [^3H]-CB binding in the absence of cytochalasins. Abscissa: [cytochalasin], μM (note the log scale). Results are shown as mean \pm SEM of at least three separate measurements made in triplicate. CB binding was measured at 50 nM [^3H]-CB. Results are shown for modulation by CB (\circ), CC (\bullet), and CH (Δ). Curves drawn through the points were computed by nonlinear regression using eq 6. The results are: CB, $K_i = K_L = 98 \pm 8.5$ nM and $\alpha = \beta = \gamma = 6.284 \pm 3.849$, $R^2 = 0.997$. CC, $K_i = 1.591 \pm 0.431$ μM , $\beta = \infty$, $\gamma = 0.433 \pm 0.003$, $R^2 = 0.986$. CH, $K_i = 98 \pm 3$ nM, $\beta = 249 \pm 45$, $\gamma = 0.449 \pm 0.019$, $R^2 = 0.94$.

parameters: K_L and α . These values are then inserted into binding eq 6, thereby simplifying nonlinear curve fitting of forskolin modulation of cytochalasin B binding (heteroinhibition) to the resolution of three parameters: K_i , β , and γ .

Table 1 summarizes the results of heteroinhibition studies in which the effects of a wide range of forskolin analogues on [^3H]-cytochalasin B binding were measured. Figure 5 and Table 1 summarize the results of similar studies in which the effects of a number of cytochalasin analogues on [^3H]-cytochalasin B binding were measured.

DISCUSSION

The human type 1 glucose transporter (GLUT1) is inhibited by diverse natural compounds. Methylxanthines and ATP act as mixed-type inhibitors of sugar exit reducing V_{\max} and increasing $K_{m(\text{app})}$.^{28–30} Cytochalasins and forskolins increase $K_{m(\text{app})}$ for exchange transport and reduce V_{\max} for net entry (see here and refs 14, 15, and 24). Tyrosine kinase inhibitors are competitive inhibitors of sugar import,³¹ and the androgens and catechins reduce V_{\max} for exit and increase $K_{m(\text{app})}$ for uptake.³² These observations are consistent with the hypothesis that cytochalasins and forskolins bind at or close to the sugar export site and that the tyrosine kinase inhibitors, androgens, and catechins bind at or close to the sugar import site.³² Methylxanthines and ATP appear to modulate transport by acting at a site(s) distinct from import and exit sites.

Recent studies have revealed an unexpected complexity in transport inhibition by import and export site ligands. When presented at very low concentrations, the exofacial site inhibitor maltose or the endofacial site inhibitors cytochalasin B (CB) or forskolin (FSK) modestly stimulate sugar import in human red blood cells.^{21,22} As inhibitor concentration is increased, sugar import stimulation is replaced by transport inhibition. The

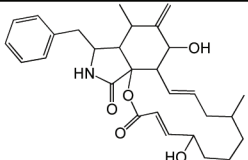
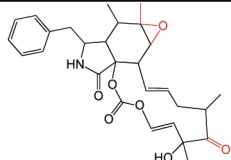
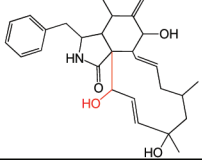
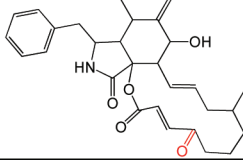
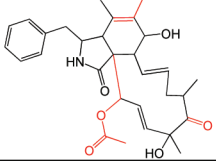
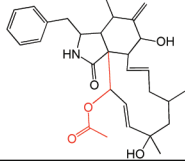
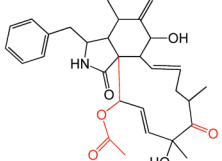
simplest explanation for this behavior is that the sugar transporter contains two binding sites for exofacial inhibitors of sugar transport and two sites for endofacial inhibitors of transport. When one exofacial or endofacial site is occupied by inhibitor, the transporter is converted into a high affinity, high capacity sugar transporter that catalyzes greater net transport.²² As the concentration of inhibitor is increased further, the second exofacial or endofacial site is occupied by inhibitor and transport is fully inhibited. The goals of the present study were to better understand the kinetics of equilibrium ligand binding at the GLUT1 export site and to explore the ligand features that determine ligand binding affinity and cooperativity.

At 4 $^{\circ}\text{C}$, where transport and ligand binding measurements were made, modulations of [^3H]-CB binding to GLUT1 by cytochalasin and forskolin analogues fall into 1 of 5 categories: type 1, *simple or pseudo-Michaelis inhibition* in which CB binding is inhibited; type 2, *schizo-modulation* in which CB binding is enhanced at low [inhibitor] but is inhibited at higher [inhibitor]; type 3, *biphasic inhibition* in which high and low affinity components of inhibition are observed; type 4, *binding stimulation* in which only enhanced binding is observed; and type 5, *no modulation of binding*. Similar ligand binding behavior has been observed with purified GLUT1 and with red cell sugar transport using a limited selection of endofacial site ligands.²¹ Type 2, 3, and 4 modulations of CB binding to GLUT1 are incompatible with the classic or alternating conformer model for carrier-mediated transport.¹⁰

This conclusion is predicated on the simplifying assumption that ligand-binding sites correspond to substrate-binding sites. For example, it is assumed that the endofacial CB binding site corresponds to (or its occupancy is mutually exclusive with) the endofacial sugar-binding site. Similarly, it is assumed that the exofacial maltose-binding site corresponds to (or its occupancy is mutually exclusive with) the exofacial sugar-binding site. How might we alter our conclusions if a simple carrier also contains noncatalytic but modulatory exo- and endofacial ligand-binding sites whose occupancy affects the affinity of substrate binding at catalytic sites? This has been considered in previous studies and rejected as a satisfactory explanation of extracellular maltose biphasic modulation of 3-*O*-methylglucose import or maltose modulation of CB binding to GLUT1.^{10,22} Moreover, if multiple ligand binding sites are presented by the endofacial conformation of GLUT1, the stoichiometry of ligand binding should be greater than 1 mol CB or FSK per mol GLUT1, and this has never been reported. However, we still do not know whether exofacial substrate and ligand binding sites are physically congruous or mutually exclusive or whether endofacial glucose, CB, and FSK binding sites are physically congruous or mutually exclusive.

The simplest explanation for these behaviors is that the sugar transporter contains 2 binding sites for endofacial transport ligands. If binding of a single ligand species is studied, interactions between binding sites are homocooperative. If binding of one ligand (e.g., [^3H]-CB or [^3H]-FSK) is measured in the presence of a second ligand, homo- and heterocooperativity may be observed. When measuring CB binding in the presence of FSK, binding of the first CB molecule to unoccupied GLUT1 is described by the dissociation constant K_L and binding of the second CB molecule is described by αK_L , where α is a dimensionless constant greater than zero. Binding of the first FSK molecule to unoccupied transporter is described by K_i , and binding of the second FSK molecule is described by βK_i (β is a dimensionless constant greater than zero). When heterocomplexes are formed, binding of the first

Table 2. Structures of the Cytochalasins^a

Cytochalasin B (CB)		Cytochalasin E (CE)	
$K_L = 0.1 \mu\text{M}$ $\beta = 6.3$ $\gamma = 6.3$		$K_L = 0.1 \mu\text{M}$ $\beta = 7917$ $\gamma = 0.56$	
Cytochalasin J (CJ)		Cytochalasin A (CA)	
$K_L = 0.01 \mu\text{M}$ $\beta = 6400$ $\gamma = 0.64$		$K_L = 0.82 \mu\text{M}$ $\beta = 1.11$ $\gamma = 0.38$	
Cytochalasin C (CC)		Cytochalasin H (CH)	
$K_L = 1.6 \mu\text{M}$ $\beta = \infty$ $\gamma = 0.43$		$K_L = 0.1 \mu\text{M}$ $\beta = 249$ $\gamma = 0.45$	
Cytochalasin D (CD)			
$K_L = 2.0 \mu\text{M}$ $\beta = 101$ $\gamma = 0.56$			

^a K_L , β , and γ are also shown (taken from Table 1) to facilitate comparison. Groups modified from the parent molecule (CB) are highlighted in red.

molecule (CB or FSK) is described by K_L or K_I and binding of the second molecule (FSK or CB) is described by γK_L or γK_I where γ is a dimensionless constant greater than zero. This model explains enhanced CB binding in the presence of at least 11 of the 20 “antagonists” tested in the present study. The following rules are observed for each type of binding modulation: Type 1: $\beta > 1$, $\gamma > 0.5$, $\beta K_I < 7200$. Type 2: $\beta < 23\,000$, $\gamma < 0.5$, $9000 < \beta K_I < 52\,000$ (the single exception is CA where $\beta K_I = 60$). Type 3: $1000 < \beta < 8000$, $\gamma > 0.5$, $150\,000 < \beta K_I < 790\,000$. Type 4: $\beta = \infty$, $\gamma < 0.5$.

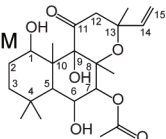
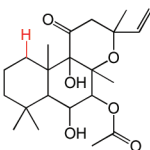
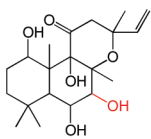
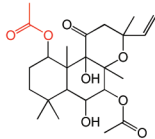
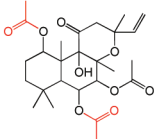
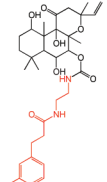
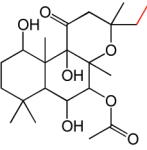
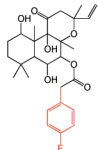
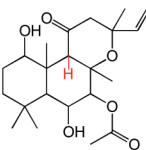
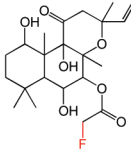
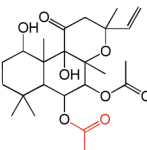
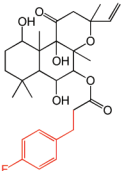
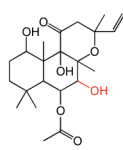
The cytochalasins (Table 2) share a common rigid bicyclic isoindoline core fused to a macrocycle. CB, CE, CH, and CJ show the greatest affinity for site 1 ($K_{d(\text{app})}$ ranges from 12 to 100 nM). Dehydration of the macrocycle hydroxyl group to form cytochalasin A (CA) results in a 60-fold loss of affinity for GLUT1 ($\Delta\Delta G^\circ = 2.28$ kcal/mol). This hydroxyl group may serve as a hydrogen bond donor. Shortening the macrocycle by three carbon atoms (CJ) increases affinity by 8-fold ($\Delta\Delta G^\circ = -1.2$ kcal/mol), but introduction of an acetyl group to the macrocycle ketone produces a compensatory 10-fold reduction in binding affinity (compare CJ and CH). Addition of a carbonyl at position 5 of the shortened macrocycle further reduces binding affinity by 20-fold (compare CD and CH). CB and CA show the highest affinities for the second binding site ($\beta K_I = 600$ and 900 nM, respectively). The remaining cytochalasins display very large β parameters indicating that they cannot simultaneously occupy endofacial sites 1 and 2. However, when site 1 is occupied by CB,

all cytochalasins have access to site 2 ($\gamma K_I = 8\text{--}1100$ nM; CC and CD share the lowest affinities for this site).

The forskolins (FSK; Table 3) are a family of labdane diterpenes known primarily for their activation of adenylyl cyclase.³³ *Schizo-modulation* of CB binding to GLUT1 is most common among the forskolins in which positions 1 and 9 are deoxygenated or where the forskolins contain small substitutions or adducts (acetylation, fluoridation) at positions 1, 6, 7, and 9. Only one forskolin derivative produces biphasic inhibition, and this contains a fluorophenylacetate group at position 7. Large changes to FSK at position 7 (deacetylation or introduction of a (2-(3-(4-fluorophenyl)-1-hydroxypropylamino)ethylamino)-methanediol group) produce *binding stimulation*, indicating that these adducts do not preclude CB binding but do prevent a second, identically modified forskolin derivative from binding. Acetylation of position 6 in combination with deacetylation of position 7 or introduction of an intermediate group at position 7 (fluorophenylpropanoic acid) appear to prevent forskolin binding altogether.

Cytochalasins and forskolins show similar heterocooperativity parameters ($\gamma = 0.49 \pm 0.06$) for binding to site 2 when site 1 is occupied by CB. This positive heterocooperativity means that forskolin or cytochalasin occupancy of site 1 increases the affinity of site 2 for CB by 2-fold, and vice versa. The exception appears to be forskolin, which displays a heterocooperativity parameter (γ) for binding to the transporter–CB complex of 0.93, suggesting

Table 3. Structures of the Forskolins^a

FSK	1DeO-FSK	7DeA-FSK	1A-FSK
$K_L = 2,800 \text{ nM}$ $\beta = 2.4$ $\gamma = 0.9$ 	$K_L = 1 \text{ nM}$ $\beta = 22000$ $\gamma = 0.44$ 	$K_L = 2 \text{ nM}$ $\beta = \infty$ $\gamma = 0.45$ 	$K_L = 3 \text{ nM}$ $\beta = 11923$ $\gamma = 0.44$ 
1,6DiA-FSK	7FPPNEA-FSK	14,15DiH-FSK	7FPA-FSK
$K_L = 11 \text{ nM}$ $\beta = 1500$ $\gamma = 0.49$ 	$K_L = 25 \text{ nM}$ $\beta = 40400$ $\gamma = 0.43$ 	$K_L = 30 \text{ nM}$ $\beta = 243$ $\gamma = 0.6$ 	$K_L = 140 \text{ nM}$ $\beta = 1120$ $\gamma = 0.51$ 
9DeO-FSK	7FA-FSK	6A-FSK	
$K_L = 430 \text{ nM}$ $\beta = 120$ $\gamma = 0.46$ 	$K_L = 630 \text{ nM}$ $\beta = 45$ $\gamma = 0.48$ 	$K_L = 950 \text{ nM}$ $\beta = 10000$ $\gamma = 0.42$ 	
7FPP-FSK	6A,7DeA-FSK		
$K_L = \text{NA}$ $\beta = \text{NA}$ $\gamma = \text{NA}$ 	$K_L = \text{NA}$ $\beta = \text{NA}$ $\gamma = \text{NA}$ 		

^a K_L , β , and γ are also shown (taken from Table 1) to facilitate comparison. Groups modified from the parent molecule (FSK) are highlighted in red.

that CB and FSK binding sites are only weakly interacting. Only 3 of 20 GLUT1 endofacial site ligands tested in the present study produce pseudo-Michaelis inhibition of CB binding. Twelve compounds enhance CB binding when applied at low concentrations. Three compounds display high and low affinity inhibition of CB binding. Only two compounds have no effect on CB binding.

Previous studies have examined cytochalasin B and forskolin inhibition of sugar transport and CB binding in human red cells^{14,25,34,35} and inhibition by cytochalasin B³⁶ or forskolin^{37,38} of energized D-galactose transport by the GalP sugar-H⁺ symport protein of *Escherichia coli*. The present study differs from previous studies in that our analysis of inhibition of ligand binding to GLUT1 allows for two interacting ligand binding sites. In their study of cytochalasin inhibition of [³H]-CB binding to red cell membranes,³⁴ Rampal and co-workers found that only CA and CB inhibit CB binding with high affinity. The remaining cytochalasins (CC through CH) were extremely low affinity inhibitors ($K_{i(\text{app})} > 100 \mu\text{M}$). While this result appears to contradict our observations, βK_i for occupation of site 2 by cytochalasin analogues in our studies corresponds to $K_{i(\text{app})}$

observed by Rampal et al.³⁴ For example, CE inhibition of CB binding is characterized by β , γ , and K_i parameters of 7900, 0.56, and 0.1 μM , respectively. If one were to analyze our data assuming a single endofacial binding site, these parameters would translate into $K_{i(\text{app})} > 1000 \mu\text{M}$. Rampal et al.³⁴ report that $K_{i(\text{app})} \geq 100 \mu\text{M}$. As with our previous studies showing that low concentrations of “inhibitors” can produce a paradoxical stimulation of transport,^{21,22} the key to the present observations is the use of inhibitor concentrations that span $K_{d(\text{app})}$ by ± 2 or more log units.

GLUT1 three-dimensional structure has been modeled using the crystal structure of *E. coli* GlpT as a homology template and human glucose-6-phosphate translocase as an “evolutionary template” to correct for missing residue assignments.¹⁶ The resulting structure has been docked with a variety of GLUT1 ligands (cytochalasin B, forskolin, glucose, galactose, mannose, quecetin, and phloretin) to reveal potential substrate binding sites.^{16,39} Salas-Burgos et al. propose that GLUT1 presents exofacial and endofacial binding sites for forskolin, phloretin, and glucose but only an endofacial site for CB. An exofacial phloretin and glucose binding site is consistent with the observed

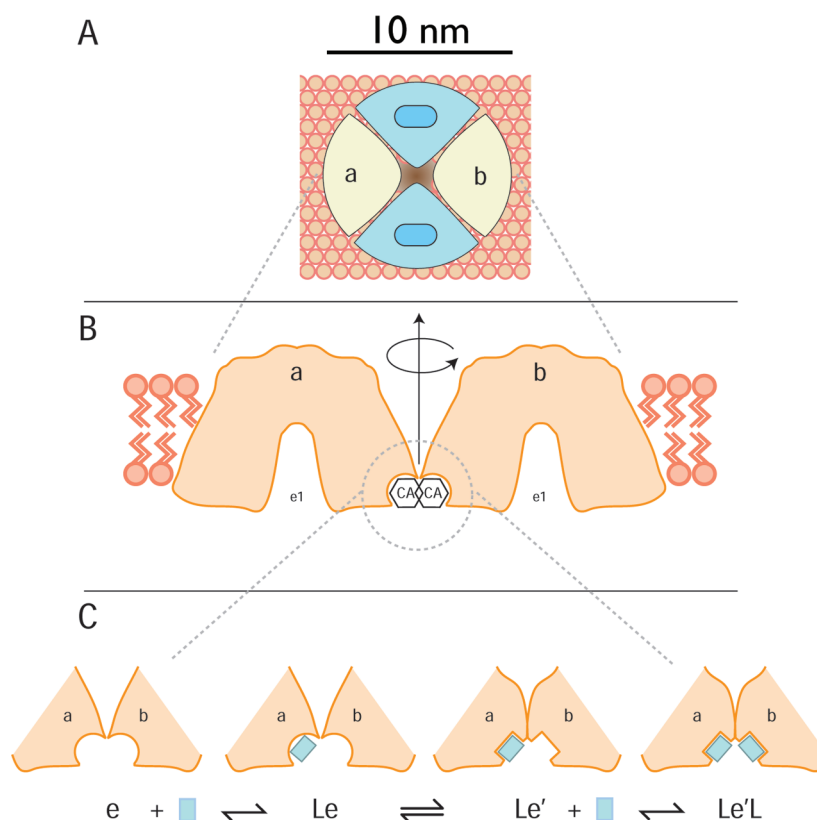


Figure 6. Panel A shows a GLUT1 tetramer (see ref 46) viewed from the interstitium. Two subunits (blue) are shown in the e2 conformation, each presenting an import site, and two subunits (a and b) are shown in the e1 conformation (their sugar binding sites are not visible because they are exposed to the cytoplasm). Panel B shows the e1 subunits a and b viewed normal to the bilayer and each sectioned directly through its catalytic center. If the GLUT1 region that binds cytochalasin B interacts with the same domain on the adjacent GLUT1 molecule (*subunit b* is rotated 180° relative to *subunit a* about the central axis of the tetramer), this would allow for the molecular envelope of a cytochalasin bound to *subunit a* to overlap with that of cytochalasin bound to *subunit b*. This, in turn, could account for strong negative cooperativity as observed, for example, with CA. Holman and Rees¹² suggest that the CB binding site lies close to TMs 10 and 11 which would require that TMs 9 and 12 most likely form the oligomerization interface. Panel C hypothesizes that ligand interaction with *subunit a* promotes a conformational change in both subunits which, in this instance, enhances the affinity of *subunit b* for ligand. However, the ligand-induced conformational change could also reduce binding affinity at *subunit b* and thereby explain negative cooperativity.

competition between substrate and phloretin during sugar uptake. However, forskolin is a noncompetitive inhibitor of sugar uptake (see here and ref 14), which is incompatible with docking analyses suggesting that exofacial glucose and forskolin compete for binding. Forskolin is proposed to make H-bond acceptor contacts with the GLUT1 endofacial site via hydroxyl or carbonyl groups at forskolin positions 6, 9, and 11. Contrary to this suggestion, elimination of the hydroxyl group at position 9 enhances ligand binding affinity. CB is proposed to dock with GLUT1 at a single site comprising portions of GLUT1 cytoplasmic loops 2, 6, and 10.¹⁶ Biochemical data suggest that CB interacts with GLUT1 transmembrane helices 10 and 11 and loop 10^{12,40,41} although the absence of a photoinduced covalent interaction between CB and loops 2 and 6 does not eliminate binding interactions with these domains. Deviations between experimental and modeled behavior are not unexpected. The use of homology-based threading to model LacY on the known GlpT structure or to model GlpT on the known LacY structure results in broadly correct transporter architecture but misaligns active site residues.⁴²

Two explanations could account for multiple, interacting endofacial ligand binding sites. (1) Both sites exist on a single GLUT1 molecule. (2) Only one site is present within each GLUT1

molecule, but GLUT1–GLUT1 interactions give rise to binding cooperativity. The first possibility is ruled out by GLUT1 CB binding stoichiometry which ranges from 0.5 to 1 mol CB per mol GLUT1.^{4,43,44} The second possibility is supported by demonstrations that GLUT1 forms noncovalent dimers and tetramers in detergent micelles and lipid bilayers (refs 44–46 but see ref 47 for a counter view). Strong, negative cooperativity could be explained if a ligand, complexed within the endofacial binding site, extends its molecular envelope into the endofacial binding pocket of an adjacent subunit, thereby inhibiting ligand binding at the second site (negative cooperativity; Figure 6 A). Positive or weak negative cooperativity would be explained if endofacial ligand binding is an induced fit phenomenon, which in turn promotes a similar or compensatory conformational change in the endofacial binding site of an adjacent GLUT1 molecule (Figure 6 B). Resolution of these questions must await determination of the structure of the GLUT1–CB complex.

The significance of GLUT1 cooperativity to GLUT1 function at physiologic temperature (37 °C) remains to be established. It has been noted that purified, reduced (noncooperative) GLUT1⁸ is some 10–20-fold less active than red cell resident GLUT1.¹ This could be explained if reduced, purified transporter behaves as a simple carrier.⁴⁵ In order that multiple rounds of sugar uptake

may proceed via a simple carrier, each transport cycle (which includes substrate binding at the exofacial surface, substrate translocation, and substrate release at the endofacial surface) must include a conformational change that restores the exofacial substrate binding site. Regeneration of the exofacial site is called relaxation¹ and, at 10 °C, is 100-fold slower than substrate translocation.⁸ Red cell resident (tetrameric) GLUT1, on the other hand, couples substrate translocation through one GLUT1 molecule to relaxation of a neighboring subunit and thereby avoids rate-limiting relaxation. The cost is significant—transport requires twice as much cooperative GLUT1 than noncooperative GLUT1—but the catalytic advantage is even greater. Studies with reduced GLUT1 at 37 °C will be necessary to determine whether insights obtained at lower temperatures are applicable to physiological temperatures. GLUT1 cooperativity has not been studied systematically in other tissues, but the hallmarks of cooperativity (GLUT1 sensitivity to reductant, interaction with quaternary-structure-sensitive polyclonal antibodies, formation of oligomers, dominant negative phenotypic behavior of heterologously expressed GLUT1 mutants) have been observed in cultured cells,^{45,48–51} suggesting that GLUT1 may behave as a cooperative complex in most tissues where it is expressed.

■ ASSOCIATED CONTENT

S Supporting Information. Details of the ligand binding model (differential equations describing Scheme 1). This material is available free of charge via the Internet at <http://pubs.acs.org>.

■ AUTHOR INFORMATION

Corresponding Author

*E-mail: Anthony.Carruthers@umassmed.edu. Tel: 508 856 5570. Fax: 508 856 6464.

Funding Sources

This work was supported by NIH grants DK 36081 and DK 44888 (A.C.). A.N.A. acknowledges a studentship from the BBSRC and support from GlaxoSmithKline plc. P.J.F.H. and R.B.H. thank the BBSRC and the EU (EDICT consortium grant 201924) for research funding.

■ ABBREVIATIONS

GLUT1, human erythrocyte glucose transport protein; CA, cytochalasin A; CB, cytochalasin B; CC, cytochalasin C; CD, cytochalasin D; CE, cytochalasin E; CH, cytochalasin H; CJ, cytochalasin J; FSK, forskolin; 1DeO-FSK, 1-deoxy-forskolin; 7DeA-FSK, 7-deacetyl-forskolin; 1A-FSK, 1-acetyl-forskolin; 1,6DiA-FSK, 1,6-diacetyl-forskolin; 7FPPNEA-FSK, 14,15DiH-FSK, 14,15-dihydro-forskolin; 7FPA-FSK, 7-fluorophenylacetyl-forskolin; 9DeO-FSK, 9-deoxy-forskolin; 7FA-FSK, 7-fluoroacetyl-forskolin; 6A-FSK, 6-acetyl-forskolin; 7FPP-FSK, 7-fluorophenylpropionate-forskolin; 6A,7DeA-FSK, 6-acetyl-7-deacetyl-forskolin; EGTA, EDTA, ethylenediaminetetraacetic acid; 3MG, 3-O-methylglucose

■ REFERENCES

- (1) Stein, W. D. (1986) Transport and diffusion across cell membranes. Academic Press, Inc: Orlando, FL, 231–305.
- (2) Saier, M. H., Jr., Beatty, J. T., Goffeau, A., Harley, K. T., Heijne, W. H., Huang, S. C., Jack, D. L., Jahn, P. S., Lew, K., Liu, J., Pao, S. S.,

Paulsen, I. T., Tseng, T. T., and Virk, P. S. (1999) The major facilitator superfamily. *J. Mol. Microbiol. Biotechnol.* 1, 257–279.

(3) Kasahara, M., and Hinkle, P. C. (1977) Reconstitution and purification of the D-glucose transporter from human erythrocytes. *J. Biol. Chem.* 252, 7384–7390.

(4) Zoccoli, M. A., Baldwin, S. A., and Lienhard, G. E. (1978) The monosaccharide transport system of the human erythrocyte. Solubilization and characterization on the basis of cytochalasin B binding. *J. Biol. Chem.* 253, 6923–6930.

(5) Takata, K., Hirano, H., and Kasahara, M. (1997) Transport of glucose across the blood-tissue barriers. *Int. Rev. Cytol., Suppl.* 172, 1–53.

(6) Pascual, J. M., Wang, D., Lecumberri, B., Yang, H., Mao, X., Yang, R., and De Vivo, D. C. (2004) GLUT1 deficiency and other glucose transporter diseases. *Eur. J. Endocrinol.* 150, 627–633.

(7) Hruz, P. W., and Mueckler, M. M. (2001) Structural analysis of the GLUT1 facilitative glucose transporter (review). *Mol. Membr. Biol.* 18, 183–193.

(8) Appleman, J. R., and Lienhard, G. E. (1989) Kinetics of the purified glucose transporter. Direct measurement of the rates of inter-conversion of transporter conformers. *Biochemistry* 28, 8221–8227.

(9) Cloherty, E. K., Heard, K. S., and Carruthers, A. (1996) Human erythrocyte sugar transport is incompatible with available carrier models. *Biochemistry* 35, 10411–10421.

(10) Sultzman, L. A., and Carruthers, A. (1999) Stop-flow analysis of cooperative interactions between GLUT1 sugar import and export sites. *Biochemistry* 38, 6640–6650.

(11) Mueckler, M., and Makepeace, C. (2004) Analysis of transmembrane segment 8 of the GLUT1 glucose transporter by cysteine-scanning mutagenesis and substituted cysteine accessibility. *J. Biol. Chem.* 279, 10494–10499.

(12) Holman, G. D., and Rees, W. D. (1987) Photolabelling of the hexose transporter at external and internal sites: fragmentation patterns and evidence for a conformational change. *Biochim. Biophys. Acta* 897, 395–405.

(13) Bloch, R. (1973) Inhibition of sugar transport in the human erythrocyte by cytochalasin B. *Biochemistry* 12, 4799–4801.

(14) Sergeant, S., and Kim, H. D. (1985) Inhibition of 3-O-methylglucose transport in human erythrocytes by forskolin. *J. Biol. Chem.* 260, 14677–14682.

(15) Carruthers, A., and Helgeson, A. L. (1991) Inhibitions of sugar transport produced by ligands binding at opposite sides of the membrane. Evidence for simultaneous occupation of the carrier by maltose and cytochalasin B. *Biochemistry* 30, 3907–3915.

(16) Salas-Burgos, A., Iserovich, P., Zuniga, F., Vera, J. C., and Fischbarg, J. (2004) Predicting the three-dimensional structure of the human facilitative glucose transporter glut1 by a novel evolutionary homology strategy: insights on the molecular mechanism of substrate migration, and binding sites for glucose and inhibitory molecules. *Biophys. J.* 87, 2990–2999.

(17) Heard, K. S., Fidyk, N., and Carruthers, A. (2000) ATP-dependent substrate occlusion by the human erythrocyte sugar transporter. *Biochemistry* 39, 3005–3014.

(18) Leitch, J. M., and Carruthers, A. (2007) ATP-dependent sugar transport complexity in human erythrocytes. *Am. J. Physiol. Cell Physiol.* 292, C974–86.

(19) Blodgett, D. M., and Carruthers, A. (2005) Quench-flow analysis reveals multiple phases of GluT1-mediated sugar transport. *Biochemistry* 44, 2650–2660.

(20) Henderson, P. J. (1972) A linear equation that describes the steady-state kinetics of enzymes and subcellular particles interacting with tightly bound inhibitors. *Biochem. J.* 127, 321–333.

(21) Cloherty, E. K., Levine, K. B., and Carruthers, A. (2001) The red blood cell glucose transporter presents multiple, nucleotide-sensitive sugar exit sites. *Biochemistry* 40, 15549–15561.

(22) Hamill, S., Cloherty, E. K., and Carruthers, A. (1999) The human erythrocyte sugar transporter presents two sugar import sites. *Biochemistry* 38, 16974–16983.

(23) Appleman, J. R., and Lienhard, G. E. (1985) Rapid kinetics of the glucose transporter from human erythrocytes. Detection and measurement of a half-turnover of the purified transporter. *J. Biol. Chem.* 260, 4575–4578.

- (24) Basketter, D. A., and Widdas, W. F. (1978) Asymmetry of the hexose transfer system in human erythrocytes. Comparison of the effects of cytochalasin B, phloretin and maltose as competitive inhibitors. *J. Physiol.* 278, 389–401.
- (25) Lavis, V. R., Lee, D. P., and Shenolikar, S. (1987) Evidence that forskolin binds to the glucose transporter of human erythrocytes. *J. Biol. Chem.* 262, 14571–14575.
- (26) Gorga, F. R., and Lienhard, G. E. (1982) Changes in the intrinsic fluorescence of the human erythrocyte monosaccharide transporter upon ligand binding. *Biochemistry* 21, 1905–1908.
- (27) Baldwin, S. A., Baldwin, J. M., and Lienhard, G. E. (1982) Monosaccharide transporter of the human erythrocyte. Characterization of an improved preparation. *Biochemistry* 21, 3836–3842.
- (28) Carruthers, A. (1989) Hexose transport across human erythrocyte membranes in *The Red Cell Membrane* (Raess, B. U., and G. Tunncliffe, G., Eds.) pp 249–279, Humana Press, Clifton, NJ.
- (29) Challiss, J. R., Taylor, L. P., and Holman, G. D. (1980) Sugar transport asymmetry in human erythrocytes—the effect of bulk haemoglobin removal and the addition of methylxanthines. *Biochim. Biophys. Acta* 602, 155–166.
- (30) Cloherty, E. K., Diamond, D. L., Heard, K. S., and Carruthers, A. (1996) Regulation of GLUT1-mediated sugar transport by an antiport/uniport switch mechanism. *Biochemistry* 35, 13231–13239.
- (31) Vera, J. C., Reyes, A. M., Velasquez, F. V., Rivas, C. I., Zhang, R. H., Strobel, P., Slebe, J. C., Nunez-Alarcon, J., and Golde, D. W. (2001) Direct inhibition of the hexose transporter GLUT1 by tyrosine kinase inhibitors. *Biochemistry* 40, 777–90.
- (32) Naftalin, R. J., Afzal, I., Cunningham, P., Halai, M., Ross, C., Salleh, N., and Milligan, S. R. (2003) Interactions of androgens, green tea catechins and the antiandrogen flutamide with the external glucose-binding site of the human erythrocyte glucose transporter GLUT1. *Br. J. Pharmacol.* 140, 487–499.
- (33) Morris, D. I., Robbins, J. D., Ruoho, A. E., Sutkowski, E. M., and Seamon, K. B. (1991) Forskolin photoaffinity labels with specificity for adenyl cyclase and the glucose transporter. *J. Biol. Chem.* 266, 13377–13384.
- (34) Rampal, A. L., Pinkofsky, H. B., and Jung, C. Y. (1980) Structure of cytochalasins and cytochalasin B binding sites in human erythrocyte membranes. *Biochemistry* 19, 679–683.
- (35) Shanahan, M. F., Morris, D. P., and Edwards, B. M. (1987) [³H]forskolin. Direct photoaffinity labeling of the erythrocyte D-glucose transporter. *J. Biol. Chem.* 262, 5978–5984.
- (36) Cairns, M. T., McDonald, T. P., Horne, P., Henderson, P. J., and Baldwin, S. A. (1991) Cytochalasin B as a probe of protein structure and substrate recognition by the galactose/H⁺ transporter of *Escherichia coli*. *J. Biol. Chem.* 266, 8176–8183.
- (37) Martin, G. E., Seamon, K. B., Brown, F. M., Shanahan, M. F., Roberts, P. E., and Henderson, P. J. (1994) Forskolin specifically inhibits the bacterial galactose-H⁺ transport protein, GalP. *J. Biol. Chem.* 269, 24870–24877.
- (38) Martin, G. E., Rutherford, N. G., Henderson, P. J., and Walmsley, A. R. (1995) Kinetics and thermodynamics of the binding of forskolin to the galactose-H⁺ transport protein, GalP, of *Escherichia coli*. *Biochem. J.* 308, 261–268.
- (39) Cunningham, P., Afzal-Ahmed, I., and Naftalin, R. J. (2006) Docking studies show that D-glucose and quercetin slide through the transporter GLUT1. *J. Biol. Chem.* 281, 5797–5803.
- (40) Kasahara, T., and Kasahara, M. (1998) Tryptophan 388 in putative transmembrane segment 10 of the rat glucose transporter Glut1 is essential for glucose transport. *J. Biol. Chem.* 273, 29113–29117.
- (41) Garcia, J. C., Strube, M., Leingang, K., Keller, K., and Mueckler, M. M. (1992) Amino acid substitutions at tryptophan 388 and tryptophan 412 of the HepG2 (Glut1) glucose transporter inhibit transport activity and targeting to the plasma membrane in *Xenopus* oocytes. *J. Biol. Chem.* 267, 7770–7776.
- (42) Lemieux, M. J. (2007) Eukaryotic major facilitator superfamily transporter modeling based on the prokaryotic GltP crystal structure (Review). *Mol. Membr. Biol.* 24, 333–341.
- (43) Jung, C. Y., and Rampal, A. L. (1977) Cytochalasin B binding sites and the glucose transporter in human erythrocyte ghosts. *J. Biol. Chem.* 252, 5456–5463.
- (44) Hebert, D. N., and Carruthers, A. (1991) Cholate-solubilized erythrocyte glucose transporters exist as a mixture of homodimers and homotetramers. *Biochemistry* 30, 4654–4658.
- (45) Zottola, R. J., Cloherty, E. K., Coderre, P. E., Hansen, A., Hebert, D. N., and Carruthers, A. (1995) Glucose transporter function is controlled by transporter oligomeric structure. A single, intramolecular disulfide promotes GLUT1 tetramerization. *Biochemistry* 34, 9734–9747.
- (46) Graybill, C., van Hoek, A. N., Desai, D., Carruthers, A. M., and Carruthers, A. (2006) Ultrastructure of Human Erythrocyte GLUT1. *Biochemistry* 45, 8096–8107.
- (47) Haneskog, L., Andersson, L., Brekkan, E., Englund, A. K., Kameyama, K., Liljas, L., Greijer, E., Fischbarg, J., and Lundahl, P. (1996) Monomeric human red cell glucose transporter (Glut1) in non-ionic detergent solution and a semi-elliptical torus model for detergent binding to membrane proteins. *Biochim. Biophys. Acta* 1282, 39–47.
- (48) Levine, K. B., Robichaud, T. K., Hamill, S., Sultzman, L. A., and Carruthers, A. (2005) Properties of the human erythrocyte glucose transport protein are determined by cellular context. *Biochemistry* 44, 5606–5616.
- (49) Levine, K. B., Cloherty, E. K., Fidyk, N. J., and Carruthers, A. (1998) Structural and physiologic determinants of human erythrocyte sugar transport regulation by adenosine triphosphate. *Biochemistry* 37, 12221–12232.
- (50) Cloherty, E. K., Sultzman, L. A., Zottola, R. J., and Carruthers, A. (1995) Net sugar transport is a multistep process. Evidence for cytosolic sugar binding sites in erythrocytes. *Biochemistry* 34, 15395–15406.
- (51) Pessino, A., Hebert, D. N., Woon, C. W., Harrison, S. A., Clancy, B. M., Buxton, J. M., Carruthers, A., and Czech, M. P. (1991) Evidence that functional erythrocyte-type glucose transporters are oligomers. *J. Biol. Chem.* 266, 20213–20217.